



RESEARCH PAPER

VCE-004.3, a cannabidiol aminoquinone derivative, prevents bleomycin-induced skin fibrosis and inflammation through PPAR γ - and CB $_2$ receptor-dependent pathways

Correspondence Eduardo Muñoz, Maimonides Biomedical Research Institute of Córdoba, University of Córdoba, Avda Menéndez Pidal s/n, 14004 Córdoba, Spain. E-mail: e.munoz@uco.es

Received 18 December 2017; **Revised** 26 June 2018; **Accepted** 12 July 2018

Carmen del Rio^{1,2,3,*}, Irene Cantarero^{1,2,3,*}, Belén Palomares^{1,2,3}, María Gómez-Cañas^{4,5,6}, Javier Fernández-Ruiz^{4,5,6} , Carolina Pavicic⁷, Adela García-Martín⁸, Maria Luz Bellido^{8,9}, Rafaela Ortega-Castro^{1,2,3}, Carlos Pérez-Sánchez^{1,2,3}, Chary López-Pedreira^{1,2,3}, Giovanni Appendino¹⁰, Marco A Calzado^{1,2,3} and Eduardo Muñoz^{1,2,3} 

¹Maimonides Biomedical Research Institute of Córdoba, University of Córdoba, Córdoba, Spain, ²Department of Cellular Biology, Physiology and Immunology, University of Córdoba, Córdoba, Spain, ³Reina Sofía University Hospital, Córdoba, Spain, ⁴Instituto Universitario de Investigación en Neuroquímica, Departamento de Bioquímica y Biología Molecular, Facultad de Medicina, Universidad Complutense, Madrid, Spain, ⁵Centro de Investigación Biomédica en Red de Enfermedades Neurodegenerativas (CIBERNED), Madrid, Spain, ⁶Instituto Ramón y Cajal de Investigación Sanitaria (IRYCIS), Madrid, Spain, ⁷Innohealth Group, Madrid, Spain, ⁸Vivacell Biotechnology, Córdoba, Spain, ⁹Emerald Health Pharmaceuticals, San Diego, CA USA, and ¹⁰Dipartimento di Scienze del Farmaco, Università del Piemonte Orientale, Novara, Italy

*Both authors contributed equally to this study.

BACKGROUND AND PURPOSE

The endocannabinoid system and PPAR γ are important targets for the development of novel compounds against fibrotic diseases such as systemic sclerosis (SSc), also called scleroderma. The aim of this study was to characterize VCE-004.3, a novel cannabidiol derivative, and study its anti-inflammatory and anti-fibrotic activities.

EXPERIMENTAL APPROACH

The binding of VCE-004.3 to CB $_1$ and CB $_2$ receptors and PPAR γ and its effect on their functional activities were studied *in vitro* and *in silico*. Anti-fibrotic effects of VCE-004.3 were investigated in NIH-3T3 fibroblasts and human dermal fibroblasts. To assess its anti-inflammatory and anti-fibrotic efficacy *in vivo*, we used two complementary models of bleomycin-induced fibrosis. Its effect on ERK1/2 phosphorylation induced by IgG from SSc patients and PDGF was also investigated.

KEY RESULTS

VCE-004.3 bound to and activated PPAR γ and CB $_2$ receptors and antagonized CB $_1$ receptors. VCE-004.3 bound to an alternative site at the PPAR γ ligand binding pocket. VCE-004.3 inhibited collagen gene transcription and synthesis and prevented TGF β -induced fibroblast migration and differentiation to myofibroblasts. It prevented skin fibrosis, myofibroblast differentiation and ERK1/2 phosphorylation in bleomycin-induced skin fibrosis. Furthermore, it reduced mast cell degranulation, macrophage activation, T-lymphocyte infiltration, and the expression of inflammatory and profibrotic factors. Topical application of VCE-004.3 also alleviated skin fibrosis. Finally, VCE-004.3 inhibited PDGF-BB- and SSc IgG-induced ERK1/2 activation in fibroblasts.

CONCLUSIONS AND IMPLICATIONS

VCE-004.3 is a novel semisynthetic cannabidiol derivative that behaves as a dual PPAR γ /CB $_2$ agonist and CB $_1$ receptor modulator that could be considered for the development of novel therapies against different forms of scleroderma.

Abbreviations

BLM, bleomycin; CB₁, cannabinoid receptor type I; CB₂, cannabinoid receptor type II; CBD, cannabidiol; ECS, endocannabinoid system; LBP, ligand binding pocket; NHDFs, normal human dermal fibroblasts; RGZ, rosiglitazone; SSc, systemic sclerosis; α -SMA, α -smooth muscle actin

Introduction

Systemic sclerosis (SSc) or scleroderma is a chronic multiorgan autoimmune disease of unknown aetiology characterized by vascular, immunological and fibrotic abnormalities. The disease is complex and dynamic, and the interrelationship among the three main hallmarks of SSc results in a wide spectrum of clinical presentations ranging from limited skin involvement [limited cutaneous SSc (lcSSc)] to widespread internal organ fibrosis [diffuse cutaneous SSc (dcSSc)]. The pathogenesis of SSc is not fully understood, and it is believed that inflammation as well as vascular injury in the initial stages drive the autoimmune response and precede fibrosis in the course of the disease (Varga and Abraham, 2007; Pattanaik *et al.*, 2015).

Several lines of evidence have shown that the endocannabinoid system (ECS) may play a role in the pathophysiology of SSc. Cannabinoids exert a broad range of biological activity including anti-inflammatory effects (Katchan *et al.*, 2016), effects on endothelial function (Bouchard *et al.*, 2003) and cell death regulation (Garcia-Gonzalez *et al.*, 2009). The ECS is composed of cannabinoid receptors, CB₁ and CB₂, their endogenous lipid ligands represented by anandamide (AEA) and 2-arachidonoylglycerol (2-AG) and the enzymes responsible for their degradation (Pacher *et al.*, 2006). CB₁ and CB₂ receptors are overexpressed in SSc fibroblasts (Garcia-Gonzalez *et al.*, 2009), and the anti-inflammatory and anti-fibrotic actions of cannabinoids have been widely demonstrated both *in vitro* and *in vivo*. Thus, inactivation of CB₁ receptors decreased the number of infiltrating T-cells and macrophages in lesioned skin (Marquart *et al.*, 2010). In contrast, CB₂ receptor activation limits leukocyte infiltration and tissue fibrosis (Akhmetshina *et al.*, 2009). Thereby, structurally different CB₂ agonists such as ajulemic acid, JHW-133 and VCE-004.8 have been shown to alleviate skin fibrosis and inflammation in experimental SSc (Akhmetshina *et al.*, 2009; Gonzalez *et al.*, 2012; del Rio *et al.*, 2016).

In addition to binding to classical CB₁ and CB₂ receptors, some natural and semisynthetic cannabinoids also bind and activate the nuclear hormone receptor PPAR γ (Pistis and O'Sullivan, 2017). PPAR γ was initially identified through its role in the regulation of glucose and lipid metabolism and cell differentiation, but it is now well established that PPAR γ agonists are also exhibit anti-inflammatory and anti-fibrotic effects (Clark, 2002; Dantas *et al.*, 2015). In this regard, PPAR γ is a regulator of connective tissue homeostasis, and different experimental approaches have shown that PPAR γ ligands attenuate hepatic (Galli *et al.*, 2002), renal (Bae *et al.*, 2017) and pulmonary fibrosis (Milam *et al.*, 2008) as well as bleomycin-induced skin fibrosis (Gonzalez *et al.*, 2012; Wei *et al.*, 2014; del Rio *et al.*, 2016; Ruzehaji *et al.*, 2016).

Different serum autoantibodies against multiple intracellular antigens have been detected and proposed as biomarkers for early and precise diagnosis in SSc (Kayser and

Fritzler, 2015). However, how autoantibodies contribute to the prognosis of SSc is not fully understood. Autoantibodies directed against non-nuclear autoantigens including anti-PDGF receptor, anti-endothelial cells, anti-fibroblast and anti-angiotensin type 1-receptor autoantibodies with possible pathogenic properties have been also described (Ho and Reveille, 2003; Baroni *et al.*, 2006; Fineschi *et al.*, 2008; Mihai and Tervaert, 2010; Kayser and Fritzler, 2015).

Hence, targeting the ECS and PPAR γ , which are considered potential therapeutic targets in SSc, represents a viable approach to prevent or attenuate inflammation and fibrosis in SSc. In the present study, we demonstrated that the novel **cannabidiol (CBD)** aminoquinone derivative VCE-004.3, which targets PPAR γ and CB₂ receptors, but also antagonizes CB₁ receptors, exhibits anti-inflammatory and anti-fibrotic effects.

Methods

Cell lines

HEK-293T, HEK-293T-CB₁, HEK-293T-CB₂, NIH-3T3 and normal human dermal fibroblasts (NHDFs) were cultured in DMEM supplemented with 10% FBS, 2 mM L-glutamine and 1% penicillin/streptomycin. All cells were maintained at 37°C and 5% CO₂ in a humidified atmosphere.

VCE-004.3 synthesis

VCE-004.3 was synthesized by oxidizing CBD with the hypervalent iodine reagent SIBX as previously described (del Rio *et al.*, 2016) and then trapping it with *n*-pentylamine (four molar equivalents) in ethanol solution (*ca.* 6 mL·mmol⁻¹ of quinone). The mixture was stirred at room temperature for 18 h, diluted with water (1:5), acidified to pH = 2 with HCl (10% aqueous solution) and then extracted with CH₂Cl₂ (30 mL). The organic layer was dried (Na₂SO₄), filtered and concentrated, and the residue was purified by reverse phase chromatography (30 at 100% CH₃CN and H₂O) to yield (1*R*,6*R*)-3-(pentylamino)-6-hydroxy-3'-methyl-4-pentyl-6'-(prop-1-en-2-yl)-[1,1'-bi(cyclohexane)]-2',3,6-triene-2,5-dione as a purple-coloured powder (*ca.* 70% yield). ¹H NMR (CDCl₃, 300 MHz) δ ppm: 6.43 (bs, 1H), 5.14 (s, 1H), 4.55 (s, 2H), 3.62 (m, 1H), 3.46 (c, *J* = 6.6 Hz, 2H), 2.72 (m, 1H), 2.48 (t, *J* = 7.7 Hz, 2H), 2.31-1.72 (m, 4H), 1.68 (s, 3H), 1.64 (s, 3H), 1.48-1.24 (m, 12H), 0.90 (m, 6H). MW: 413.61.

Binding assay

PPAR γ binding activity was measured by using a PolarScreen™ PPAR Competitor Assay Kit (Life Technologies, Carlsbad, CA, USA) following the manufacturer's instructions. IC₅₀ values were calculated using GraphPad Prism. Binding affinities to cannabinoid receptors were tested by competition studies using commercial membranes

containing HEK293 EBNA cells stably expressing human CB₁ or CB₂ receptors (Perkin-Elmer Life and Analytical Sciences, Boston, MA, USA). Inhibition of [³H]-CP55940 binding was measured following a previously described procedure (Ragusa *et al.*, 2015). Competition binding data were analysed by using GraphPad Prism[®] version 5.01 (GraphPad Software Inc., CA, USA).

Docking analysis

Docking analysis was performed using *AutoDock4* (Morris *et al.*, 2009) and *Vina* softwares (Trott and Olson, 2010) with the virtual screening tool *PyRx* (Wolf, 2009) and *PyMOL* (Baugh *et al.*, 2011). The receptor model used was the Protein Data Bank (PDB) reference (RCSB PDB accession code), 3B0R (Hughes *et al.*, 2014), and 5U5L (Rajapaksha *et al.*, 2017). The search space for the docking was set according to previous findings about several binding sites for different ligands. After analysis, *AutoDock Vina* provides the estimated binding affinity value, which is the sum of the intermolecular energy and the torsional free-energy penalty. A negative value indicates that a bond is thermodynamically stable, whereas a positive value means it is unstable. Search space for the docking was set around the binding sites described previously (Hughes *et al.*, 2014).

Cytotoxicity assay

NIH-3T3 (1×10^3 cells) were seeded in 96 well plates and after 24 h incubated with VCE-004.3 for another 6 h in the presence of 0.1 μ M YOYO-1 (Life Technologies). The survival of untreated cells was considered to be 100%. Fluorescence was measured using an Incucyte FLR imaging system (Essen BioScience, Ann Arbor, MI, USA).

Transfections and luciferase assays

HEK-293T (8×10^4) cells stably expressing human cannabinoid CB₁ or CB₂ receptors were seeded in 24-well plates and after 24 h were transiently transfected with the pCRE-luc plasmid (0.2 μ g per well) using Roti[®]-Fect (Carl Roth, Karlsruhe, Germany) following the manufacturer's instructions. The cAMP response element (CRE) luciferase reporter contains the firefly luciferase gene under the control of multimerized CRE located upstream of a minimal promoter. Twenty-four hours after transfection, CB₁-HEK-293T cells were pretreated for 30 min with VCE-004.3 and stimulated with WIN55,212 (1 μ M) for 6 h. CB₂-HEK-293T cells were pretreated for 30 min with VCE-004.3 or WIN55,212 as positive control and stimulated with forskolin (10 μ M) for 6 h. NIH-3T3 (5×10^4) cells were seeded in 24-well plates and after 24 h were transiently transfected with the indicated constructs (PPAR γ -GAL4, 0.2 μ g; PPAR α -GAL4, 0.2 μ g; PPAR δ -GAL4, 0.2 μ g; GAL4-luc, 0.8 μ g; or CAGA-luc, 0.5 μ g). NIH-3T3 stably expressing Col1A2-luc were seeded in 24-well plates (5×10^4 cells per well) and treated as indicated. After treatments, luciferase activity was measured using a Dual-Luciferase Assay (Promega, Madison, WI, USA).

Measurement of collagen secretion and accumulation

NHDFs were seeded in 24-well plates (5×10^4 cells per well), pretreated with VCE-004.3 for 1 h and stimulated with

TGF β 1 for the following 24 h. The deposits of collagen were determined by measuring absorbance at 540 and 605 nm in a Genesis 10 UV spectrophotometer after cells had been stained for 30 min with a mixture of 0.1% Sirius Red and 0.1% Fast Green in saturated picric acid. Collagen secretion was studied by collecting culture medium and measuring soluble collagen using the Sircol Soluble Collagen Assay (Biocolor, County Antrim, UK) following the manufacturer's instructions.

Western blot

Cells were seeded in 6-well plates (1.5×10^5 cells) or in 60 mm plates (3×10^5 cells). After the various treatments, cells were washed with PBS and proteins extracted in 50 μ L of lysis buffer (50 mM Tris-HCl pH 7.5, 150 mM NaCl, 10% glycerol and 1% NP-40) with 10 mM NaF, 1 mM Na₃VO₄, 10 μ g·mL⁻¹ leupeptine, 1 μ g·mL⁻¹ pepstatin and aprotinin and 1 μ L·mL⁻¹ saturated PMSF; 30 μ g of proteins were boiled at 95°C in Laemmli buffer and electrophoresed in 10% SDS/PAGE gels. Separated proteins were transferred (20 V for 30 min) to PVDF membranes and blocked in 0.1% Tween 20 in TBS solution containing 5% skimmed milk for 1 h at room temperature. Membranes were incubated with primary antibodies against pSMAD2 (1:500; AB3849, Merck Millipore, Billerica, MA, USA), SMAD2 (1:1000; Cat # 5339, Cell Signalling, Danvers, MA, USA), p-ERK1/2 (1:500; sc-7383, Santa Cruz Biotechnology, Dallas, TX, USA) and ERK 1/2 (1:2000; M5670, Sigma, St Louis, MO, USA) overnight at 4°C. Membranes were washed and incubated with the appropriate HRP-conjugated secondary antibody for 1 h at room temperature and detected by chemiluminescence system (GE Healthcare Europe GmbH, Freiburg, Germany). Blots were normalized to those obtained with antibodies against α -tubulin or β -actin (1:10 000; DM-1A and AC-74, Sigma). Densitometric analysis was performed with ImageJ software (NIH, Bethesda, MD, USA).

Cell migration assay

NHDFs (2×10^3 cells) were seeded in complete DMEM in a 96-well Essen ImageLock plates (Essen BioScience). When cells reached confluence, wounds were made by scratching using the 96-pin WoundMaker (Essen BioScience). Then, culture medium was replaced by DMEM supplemented with 1% antibiotics and with mitomycin C (10 ng·mL⁻¹) to block cell proliferation. VCE-004.3 and TGF β 1 10 ng·mL⁻¹ were added in parallel. Wound healing activity was analysed using IncuCyte HD system by taking images every 3 h for 48 h and the percentage of wound confluence calculated with the IncuCyte software.

Fibroblast to myofibroblast differentiation

NIH-3T3 cells (1.5×10^4) were seeded onto glass coverslips or directly in 6-well plates. Cells were serum starved (1% FBS) for 24 h, pre-stimulated with RGZ (rosiglitazone) or VCE-004.3 for 1 h and incubated with 10 ng·mL⁻¹ TGF β 1 for 24 h. Then, cells were washed with PBS for further Western blot analysis or fixed with 4% formaldehyde for 10 min at 37°C. After fixation, cells were washed twice with PBS and blocked in IHC selective blocking reagent (Merck Millipore) for 30 min. Cells were incubated overnight at 4°C with the primary antibody for α -smooth muscle actin (α -SMA) (1:50 in blocking solution,

sc-32 251, Santa Cruz), washed three times with PBS containing 0.1% Tween 20 and incubated with the secondary antibody goat anti-rat coupled to Alexa 488 (1:1000, Merck Millipore) for 3 h at room temperature. Coverslips were mounted with Vectashield Mounting Medium supplemented with DAPI for nuclear staining. Observations were carried out using a Leica DM2500 microscope and Leica DFC420c camera. Images were acquired as sets of colour images and prepared using ImageJ software.

Animal experiments

Animal studies are reported in compliance with the ARRIVE guidelines (Kilkenny *et al.*, 2010; McGrath and Lilley, 2015). A total of 90 BALB/C female mice (6–8 weeks old) weighing between 17 and 20 g (Envigo, Valencia, Spain) were used in the studies. Experiments were performed in accordance with European Union guidelines and were approved by the Animal Research Ethic Committee of Córdoba University and the Andalusian Committee for Animal Experimentation (2014PI/016). Mice were housed in groups of nine animals in polycarbonate cages (300 mm × 180 mm × 150 mm) with free access to food and water, in the animal facilities of the University of Córdoba, and maintained in a 12 h light/dark cycle with controlled temperature (20 ± 2°C) and relative humidity (40–50%) (McGrath and Lilley, 2015).

Different administration schedules of s.c. bleomycin (BLM) have been widely used as SSc models. Repetitive injections of s.c. BLM induce skin fibrosis localized to the injection area and lead to systemic symptoms such as lung fibrosis (Beyer *et al.*, 2010). Two different BLM-induced models were used to assess the effects of VCE-004.3 *in vivo*. (i) The inflammatory model of SSc was used to study the preventive effects of VCE-004.3. Fibrosis was induced by daily s.c. administration of BLM (50 µg per mice; 100 µL) (Mylan, Barcelona, Spain) for 3 weeks. Treatments were administered in parallel and consisted of daily i.p. injections of VCE-004.3 (20 mg·kg⁻¹), RGZ (5 mg·kg⁻¹) or vehicle (4% DMSO, 6.2% Tween 20, saline; 100 µL). S.c. injections of 0.9% NaCl served as a control. (ii) A pre-established fibrosis model of SSc was induced to study the curative effect of VCE-004.3. Fibrosis was induced by daily s.c. injections of BLM (20 µg per mice; 100 µL) for 6 weeks. After 3 weeks of BLM administration, animals were treated in parallel with a daily i.p. injection of VCE-004.3 (20 mg·kg⁻¹), RGZ (5 mg·kg⁻¹) or vehicle or were given topical application of VCE-004.3 (250 µM) or vehicle (7:3 polypropylene glycol : ethanol; 100 µL) for the remaining 3 weeks. Mice were acclimatized to manipulators for a week before the experiments in order to reduce stress and allow the detection of subtle changes in behaviour by researchers. Mice weight was evaluated weekly, and no significant changes were observed between experimental groups. No behavioural changes were observed during the protocols. Neither piloerection nor hunched appearances were apparent during the experimental procedures. Mice were killed by cervical dislocation, and the back skin was removed and processed for histological examination or was frozen for further analysis. Macroscopic evaluation of internal organs did not reveal any pathological changes.

Blinding and randomization

Laboratory animals were randomly assigned to experimental groups, and treatments were assessed by a blinded investigator. The order of treatment administration was also randomized. All animal samples were studied, and analysis was carried out in a blinded manner. For immunohistochemical studies, three random fields of each skin biopsy were photographed and evaluated by two independent observers.

Histochemical analysis

Skin sections (5 µm-thick) were stained with Masson's trichrome, picosirius red or toluidine blue. Myofibroblasts were detected in skin sections by immunofluorescent labelling with α -SMA (1:50, sc-32 251, Santa Cruz) and Alexa 488 (A-11008; Life Technologies). For quantification, images were taken with a LSM 5 Exciter confocal microscope (Zeiss, Jena, Germany) and quantified in 10 to 15 randomly chosen fields at 250 magnification using ImageJ software (<http://rsb.info.nih.gov/ij>). For immunohistochemical detection of macrophages, T-cells and ERK1/2 activation, we used F4/80 (1:50; MCA497, Bio-Rad), CD3 (1:100, sc20047, Santa Cruz) and p-ERK 1/2 (1:100; sc-7383, Santa Cruz) antibodies respectively. Slides were developed with diaminobenzidine chromogen (Merck Millipore) and counterstained with Harris haematoxylin solution. Slides were photographed, digitized using a Leica DFC420c camera and analysed using ImageJ software.

Real-time PCR

Total RNA was isolated from mice frozen skin tissue using QIAzol Lysis Reagent (Qiagen, Hilden, Germany) and purified with RNeasy Mini Kit (Qiagen). Total RNA (1 µg) was retrotranscribed using the iScript™ cDNA Synthesis Kit (Bio-Rad), and the cDNA generated was analysed by real-time PCR using the iQTM SYBR Green Supermix (Bio-Rad) using a CFX96 Real-Time PCR Detection System (Bio-Rad). The oligonucleotide primers used are listed in Supporting Information Table S1. Gene expression was normalized to GAPDH mRNA levels in each sample and expressed using the 2^{- $\Delta\Delta C_t$} method.

Patients and IgG antibodies purification

In total, 12 patients, six with lSSc and six with dSSc, were included in the study after ethics committee approval. All subjects provided written informed consent. Samples were obtained from peripheral venous blood. IgGs were purified using a pool of six patients with lSSc and six patients with dSSc using high affinity chromatography of G-sepharose protein (MabTrap, GE Healthcare Bio-Sciences AB, Uppsala, Sweden) following the manufacturer's recommendations.

Data and statistical analysis

The data and statistical analysis comply with the recommendations on experimental design and analysis in pharmacology (Curtis *et al.*, 2018). *In vitro* results are shown as mean ± SD and *in vivo* data as mean ± SEM. Statistical analysis was carried out using the SPSS v.19 software for Windows (IBM Corporation, New York, USA). Results were tested for normal distribution using Kolmogorov–Smirnov normality test. Then, data were analysed using one-way ANOVA

followed by Tukey's *post hoc* test when F achieved was $P < 0.05$, and there was no significant variance in homogeneity. Some results were normalized to control to avoid unwanted sources of variation. Differences between not normally distributed results were studied by the Kruskal–Wallis followed by Dunn's *post hoc* test using the GraphPad Prism v.5 for Windows. Minimal statistical significance was set at $P < 0.05$.

Materials

Rosiglitazone (RGZ) was from Cayman Chem (Ann Arbor, MI, USA), TGF β 1 was obtained from Immunotools GmbH (Friesoythe, Germany) and non-immunized human IgG was from Jackson ImmunoResearch (West Grove, PA, USA). All other reagents were purchased from Sigma Co (St Louis, MO, USA).

Nomenclature of targets and ligands

Key protein targets and ligands in this article are hyperlinked to corresponding entries in <http://www.guidetopharmacology.org>, the common portal for data from the IUPHAR/BPS Guide to PHARMACOLOGY (Harding *et al.*, 2018) and are permanently archived in the Concise Guide to PHARMACOLOGY 2017/18 (Alexander *et al.*, 2017a,b,c).

Results

VCE-004.3 is a CBD quinone derivative with selective PPAR γ and CB $_2$ agonism and CB $_1$ antagonism

We have previously shown that VCE-004.8, a dual PPAR γ /CB $_2$ agonist, alleviates dermal fibrosis through PPAR γ and CB $_2$ receptor-dependent pathways in a mice model of SS (del Rio *et al.*, 2016). As part of our programme of chemical synthesis searching for CBD quinone derivatives, we selected the novel compound VCE-004.3 (Figure 1A) and investigated its mechanism of action and efficacy in dermal inflammation and fibrotic events. Firstly, we evaluated the binding affinity to PPAR γ and found that VCE-004.3 was able to bind PPAR γ with an IC $_{50}$ of 3.5 μ M, which is a significantly lower affinity than the binding of RGZ (Figure 1B). VCE-004.3 was not cytotoxic and induced PPAR γ transcriptional activity in a concentration-dependent manner in NIH-3T3 cells transiently co-transfected with GAL4-luc and PPAR γ -GAL4 plasmids (Figure 1C). However, VCE-004.3 did not activate PPAR α (Figure 1D) or PPAR δ (Figure 1E) transcription, indicating that VCE-004.3 is a selective agonist of the PPAR γ isoform.

To further characterize the effects of VCE-004.3 on PPAR γ transcriptional activities, we performed experiments to study the behaviour of VCE-004.3 in the presence of RGZ. To this end, GAL4-PPAR γ /GAL4-luc transfected NIH-3T3 cells were preincubated with increasing concentrations of VCE-004.3 and then treated with 1 μ M RGZ. VCE-004.3 decreased the RGZ-induced PPAR γ transactivation (Figure 2A), suggesting that VCE-004.3 could prevent RGZ binding by competing with the same binding site on PPAR γ . Moreover, the stimulating effect on PPAR γ was eliminated after removal of VCE-004.3 by washing cells with PBS, suggesting that VCE-004.3

binds to PPAR γ in a reversible and non-covalent manner (Figure 2B).

It was previously reported that synthetic PPAR γ ligands bind to the canonical ligand binding pocket (LBP) and also to an alternate site on this nuclear receptor, an effect that cannot be blocked by covalently bound synthetic antagonists, demonstrating non-overlapping binding with the canonical pocket (Hughes *et al.*, 2014). Therefore, we performed docking experiments using crystal structures 3BOR and 5U5L deposited in the PDB. As depicted in Figure 2C, molecular docking with 3BOR indicated that VCE-004.3 binds Leu 340 in Ω -loop β 3 and Tyr 373 in Helix 1/2 (alternative site) with a predicted K_i of 108.38 nM. In the presence of GW9662 in the canonical site, VCE-004.3 binds to Ser 342 in the Ω -loop β 3– β 4 and Leu 340 in β 3 with a predicted K_i of 569.80 nM. In the case of 5U5L, VCE-004.3 was found to bind Ser 342 in the Ω -loop β 3– β 4 and Gly 346 in β 4 with a predicted K_i of 1.12 μ M, and in the presence of GW9662, we found that VCE-004.3 binds to Leu 340 in β 3 and Ser 342 in Ω -loop β 3– β 4 with a predicted K_i of 17.72 nM.

To confirm that VCE-004.3 is functional through the alternative binding site, we studied VCE-004.3-mediated PPAR γ transcriptional activity in the presence of T0070907, an irreversible PPAR γ antagonist that covalently binds to Cys 285 in the PPAR γ LBP canonical binding site. As expected, T0070907 was very effective at blocking RGZ-induced PPAR γ transactivation (Figure 2D), which is consistent with the fact that RGZ activates PPAR γ by acting mainly through the canonical binding site (Hughes *et al.*, 2014). By contrast, T0070907 did not block the transcriptional activity of VCE-004.3 (Figure 2E). Altogether, our results strongly suggest that, in contrast to RGZ, VCE-004.3 is a PPAR γ modulator (m-PPAR γ) acting preferentially through the PPAR γ LBP alternative binding site. In this sense, human mesenchymal stem cells treated with VCE-004.3 showed fewer and smaller lipid droplets and lower expression levels of adipogenic differentiation markers such as PPAR γ , ADIPOQ and CEBPA compared to cells treated with the PPAR γ full agonist (PPAR γ -fa) RGZ (Supporting Information Figure S1).

Next, we studied the effect of VCE-004.3 on CB $_1$ and CB $_2$ receptors. VCE-004.3 was able to bind CB $_1$ receptors with a p K_i value of 5.61 \pm 0.15 (Figure 3A) and antagonized the activity of WIN55,212 in HEK293T-CB $_1$ cells transfected with the pCRE-luc reporter plasmid (Figure 3B). VCE-004.3 also bound to CB $_2$ receptor-containing membranes with a p K_i value of 6.69 \pm 0.10 (Figure 3C) behaving as CB $_2$ agonist since it inhibited forskolin-induced luciferase activity in HEK293T-CB $_2$ cells transfected with the pCRE-luc reporter plasmid (Figure 3D). The effects of WIN55,212 and VCE-004.3 on CB $_2$ receptor activation were prevented by the CB $_2$ antagonists AM630 and SR144528 (data not shown). In summary, VCE-004.3 is a dual PPAR γ /CB $_2$ agonist with CB $_1$ antagonistic activity.

VCE-004.3 prevented collagen transcription and synthesis induced by TGF β

It has been shown that PPAR γ ligands inhibit TGF β -induced collagen gene transcription by targeting the p300 transcriptional coactivator (Ghosh *et al.*, 2009). Thus, we studied the effect of VCE-004.3 on collagen transcription in NIH-3T3

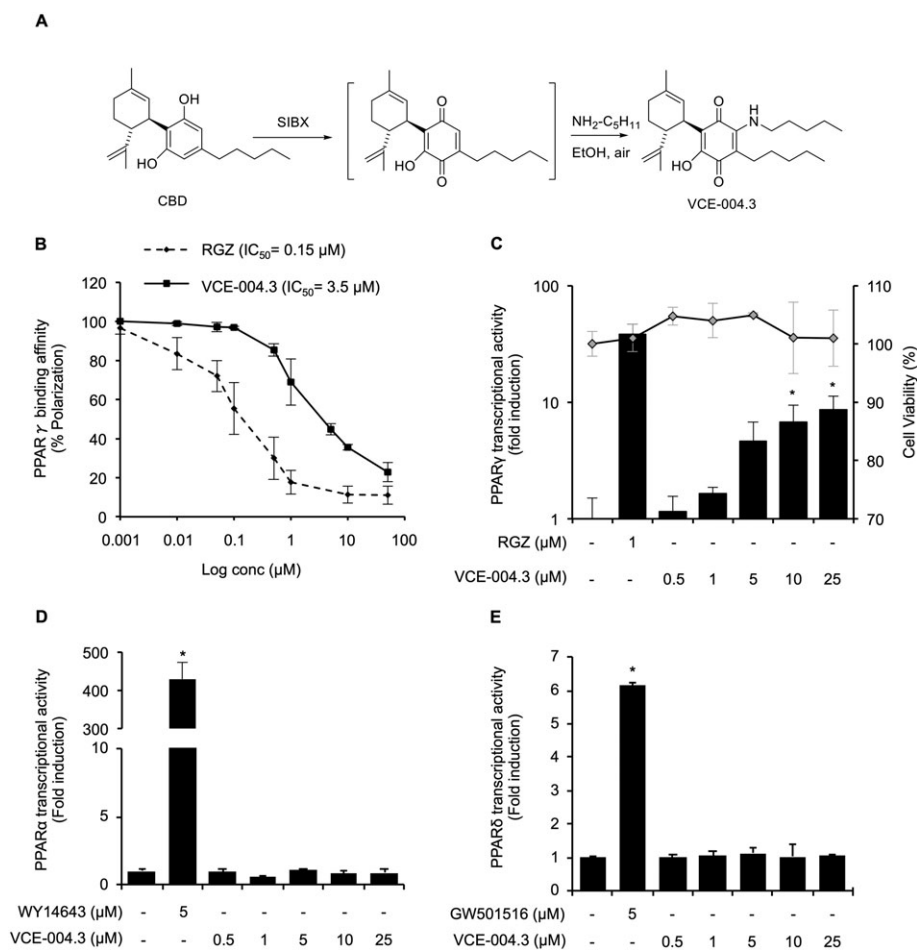


Figure 1

VCE-004.3 is a selective PPAR γ agonist. (A) Schematic for synthesis of VCE-004.3. (B) The binding affinity of VCE-004.3 and RGZ to PPAR γ . Results are presented as a logarithmic scale, and IC₅₀ values were calculated as the 50% inhibition of percentage of fluorescence polarization ($n = 5$). (C) PPAR γ transcriptional activity induced by VCE-004.3 its cytotoxicity in NIH-3T3 fibroblasts. Cells were co-transfected with PPAR γ -GAL4 and GAL4-luc constructs, stimulated with VCE-004.3 or RGZ as a positive control for 6 h and lysed for luciferase activity. Results are presented in a bar chart and shown as fold induction compared to control ($n = 10$). To test cytotoxicity, cells were treated with the compound for 6 h in the presence of YOYO-1, and fluorescence intensity was measured and presented in a dot chart ($n = 5$). (D and E) HEK-293T cells were co-transfected with PPAR α -GAL4 (D) or PPAR δ -GAL4 (E) and GAL4-luc, treated with VCE-004.3 for 6 h and lysed for luciferase activity ($n = 5$). Results are shown as mean \pm SD. * $P < 0.05$ versus control.

cells stably expressing the Col1A2-luc plasmid, which encodes the gene promoter of the pro- α 2 chain component of type I collagen fused to the luciferase gene. Pretreatment with either RGZ or VCE-004.3 resulted in a significant inhibition of collagen transcription induced by TGF β 1 stimulation (Figure 4A). The binding of TGF β to its receptor entails the activation of SMAD2/SMAD3 by phosphorylation, induction of its transcriptional activity and stimulation of the Col1A2 promoter (Shi and Massague, 2003). Pre-incubation of NIH-3T3 cells transfected with CAGA-luc plasmid with VCE-004.3 significantly reduced SMAD's transcriptional activity (Figure 4B). To further investigate the effect of VCE-004.3 on TGF β 1 signalling, we studied both the canonical and the ERK1/2 non-canonical pathways. As depicted in Figure 4C, VCE-004.3 did not interfere with TGF β 1-induced SMAD2 phosphorylation, but it inhibited the phosphorylation of ERK1/2 proteins in NIH-3T3 cells. Similar results were found

with RGZ. Next, to correlate the effect of VCE-004.3 on Col1A2 transcriptional activity with collagen secretion and deposition, NHDFs were preincubated with increasing concentrations of VCE-004.3 and stimulated with TGF β 1 for 24 h. VCE-004.3 significantly inhibited TGF β 1-induced collagen release and accumulation in NHDFs (Figure 4D, E).

VCE-004.3 prevented BLM-induced dermal inflammation and fibrosis in vivo

The BLM mice model is widely used to evaluate potential anti-inflammatory and anti-fibrotic therapies for SSc (Wu *et al.*, 2009; Gonzalez *et al.*, 2012; del Rio *et al.*, 2016; Ruzehaji *et al.*, 2016). BLM causes inflammation in a short period of time, characterized by an elevation of pro-inflammatory cytokines and growth factors that peak around day 14 of BLM exposure (Avouac, 2014). In this model of inflammation,

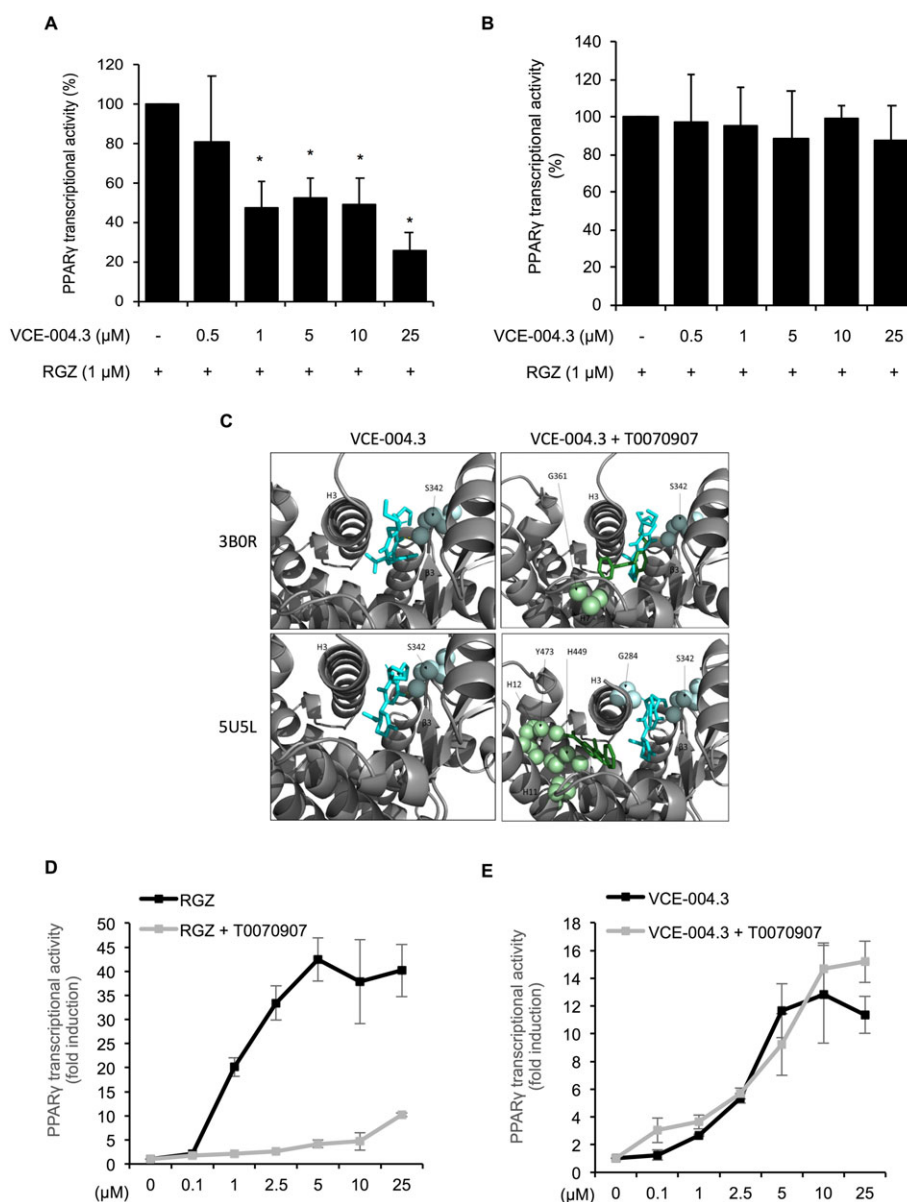


Figure 2

VCE-004.3 competed with RGZ for the canonical pocket and binds to an alternate site in PPAR γ . NIH-3T3 cells were transfected with PPAR γ -GAL4 plus GAL4-luc. (A) Cells were pretreated with VCE-004.3 for 1 h and then incubated for 6 h in the presence of RGZ ($n = 5$). (B) Cells were pretreated with VCE-004.3 for 1 h and then washed with PBS and stimulated with RGZ for 6 h ($n = 5$). (C) PPAR γ LBD structures 3BOR and 5U5L bound to VCE-004.3 (blue) with and without GW9662 (orange). (D and E) NIH-3T3 cells were transfected with PPAR γ -GAL4 plus GAL4-luc, pretreated with T0070907 (5 μ M) for 30 min and stimulated with RGZ (D) or VCE-004.3 (E) for 6 h ($n = 5$). Cells were lysed and tested for luciferase activity. Results are shown as mean \pm SD. * $P < 0.05$ versus untreated cells.

BLM administration for 3 weeks resulted in increased dermal thickness versus the control group, which was attenuated by RGZ and VCE-004.3 treatments. However, neither RGZ nor VCE-004.3 was able to restore the loss of adipose tissue layer induced by BLM administration (Figure 5A). In addition, RGZ as well as VCE-004.3 were able to reduce collagen accumulation in the skin after BLM administration (Figure 5B). Next, we studied the expression of cytokines associated with inflammation and fibrosis. As expected, BLM-treated mice had significantly higher expression levels of *IL-4*, *IL-6* and

Ccl2 in the skin compared with control mice. This up-regulation was significantly reduced in mice treated with either RGZ or VCE-004.3 (Figure 5C). Despite no significant changes in the expression levels of *IL-1 β* , *Tgfb β* and *IL-13* observed after BLM challenge, the expression of these cytokines was less in mice treated with RGZ or VCE-004.3 (Figure 5C).

Mast cell degranulation as well as macrophage and lymphocyte accumulation are the hallmarks of BLM-induced fibrosis and play important roles during the inflammatory phase of SSc (Yamamoto *et al.*, 1999). Toluidine blue staining

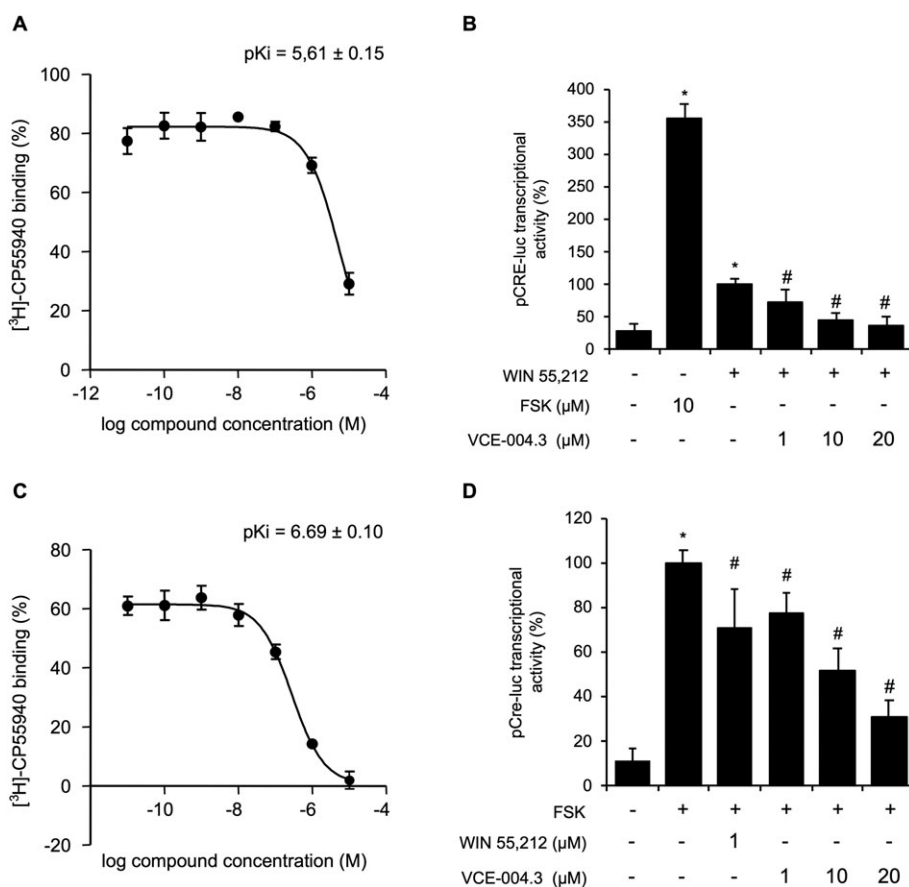


Figure 3

VCE-004.3 is a functional CB₁ antagonist and CB₂ agonist. (A) VCE-004.3 binding affinity to CB₁ receptor membranes. Results are expressed as mean \pm SEM ($n = 5$). (B) CB₁ receptor antagonism. HEK293-T-CB₁ cells transfected with pCRE-luc plasmid were pretreated for 30 min with VCE-004.3, stimulated with WIN55,212 (1 μ M) for 6 h and lysed for luciferase activity. Results are expressed as mean \pm SD ($n = 5$). (C) Binding affinity of VCE-004.3 to CB₂ receptor membranes. Results are presented as mean \pm SD ($n = 5$). (D) VCE-004.3 is a functional CB₂ receptor agonist. HEK293-T cells stably expressing CB₂ receptors were transfected with pCRE-luc plasmid and pretreated for 30 min with VCE-004.3 or WIN55,212 as positive control. Then, cells were stimulated with forskolin (FSK; 10 μ M) for 6 h and lysed for luciferase activity. Results are shown as mean \pm SD ($n = 5$). * $P < 0.05$ versus untreated cells. # $P < 0.05$ versus positive control.

showed an increased number of degranulated mast cells in the lesioned skin of the BLM group. Although we did not observe any effect in the RGZ-treated group, treatment with VCE-004.3 significantly decreased mast cell degranulation to levels comparable to the control group. Moreover, immunohistochemical examination demonstrated that VCE-004.3 significantly reduced the infiltration of F4/80⁺ macrophages and CD3⁺ lymphocytes compared with BLM untreated mice (Figure 6).

It is well known that TGF β drives the conversion of fibroblasts into myofibroblasts, and the accumulation of myofibroblasts in fibrotic skin is a hallmark of SSc (Gilbane *et al.*, 2013; Marangoni *et al.*, 2015). Myofibroblasts are characterized by the *de novo* synthesis of α -SMA fibres, and we found a substantial reduction of spindle-shaped α -SMA⁺ cells populating the fibrotic dermis from the RGZ and VCE-004.3 treated groups (Figure 7A). Moreover, VCE-004.3, as well as RGZ, prevented the changes in cell morphology including cellular hypertrophy and cell shape variations from stellate to bipolar cells associated with TGF β 1-induced myofibroblast differentiation (Figure 7B). This was accompanied by a

reduction in the steady levels of α -SMA protein; this effect was statistically significant at the dose of 10 μ M (Figure 7C) and indicated that PPAR γ ligands such as VCE-004.3 attenuate TGF β -induced myofibroblast differentiation.

It has been previously shown that disruption of the MAPK/ERK pathway reduces inflammation and fibrosis *in vivo* (Galuppo *et al.*, 2011). Therefore, we evaluated the status of phosphorylated ERK1/2 in the skin after BLM administration. Mice subjected to BLM administration showed a significant increase in ERK1/2 phosphorylation while treatment with VCE-004.3 as well as RGZ resulted in a significant decrease in p-ERK1/2 immunostaining (Figure 8).

VCE-004.3 alleviated established fibrosis in mice

To evaluate the efficacy of VCE-004.3 in a model of established skin fibrosis, mice were challenged with BLM for 6 weeks, and the pharmacological treatments were carried out during the last 3 weeks of BLM injections. Animals were treated with BLM alone, BLM plus RGZ (5 mg·kg⁻¹ i.p.), BLM

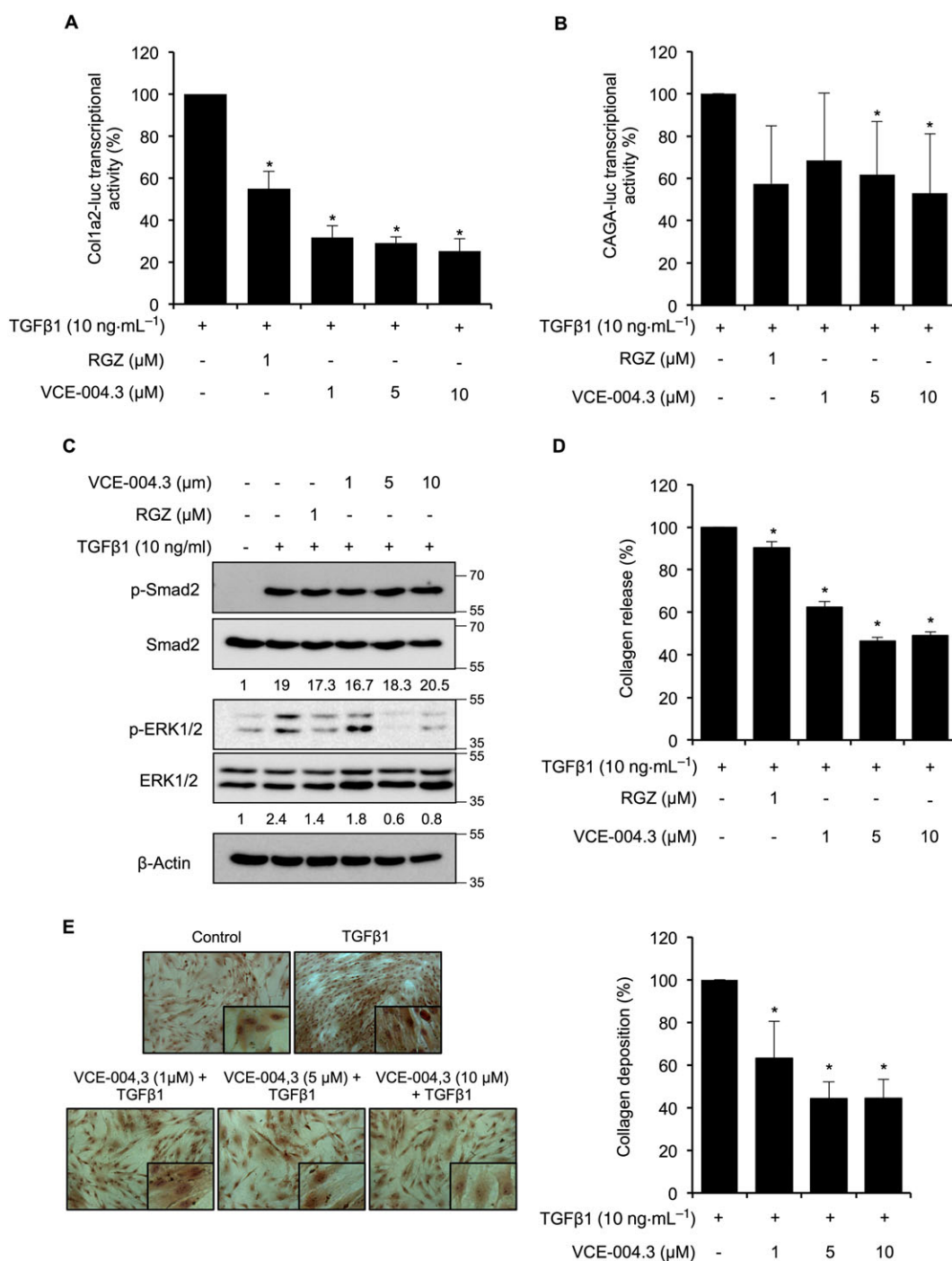


Figure 4

Effect of VCE-004.3 on collagen gene transcription and synthesis *in vitro*. (A) NIH-3T3-Col1A2-luc cells were pretreated with VCE-004.3 for 1 h and stimulated with TGFβ1 for the following 24 h ($n = 5$). (B) NIH-3T3 cells were transfected with CAGA-luc plasmid, pretreated with VCE-004.3 for 1 h and stimulated with TGFβ1 for 6 h ($n = 5$). Cells were tested for luciferase activity. (C) Serum-starved NIH-3T3 cells were preincubated with the compound for 1 h and stimulated with TGFβ1 for 2 h. Protein expression was studied by Western blot, and values under images represent mean fold induction of signal intensities after β-actin normalization ($n = 5$). (D and E) NHDFs were serum starved (1% FBS) for 24 h. Then, cells were pretreated with VCE-004.3 for 1 h and stimulated with TGFβ1 for 24 h. Soluble collagen in the culture medium was measured using the Sircol Assay (D), and collagen deposits were studied by the Sirius Red method (E). Results are presented as mean percentage of inhibition ± SD taking TGFβ1 alone as 100%. * $P < 0.05$ versus TGFβ1.

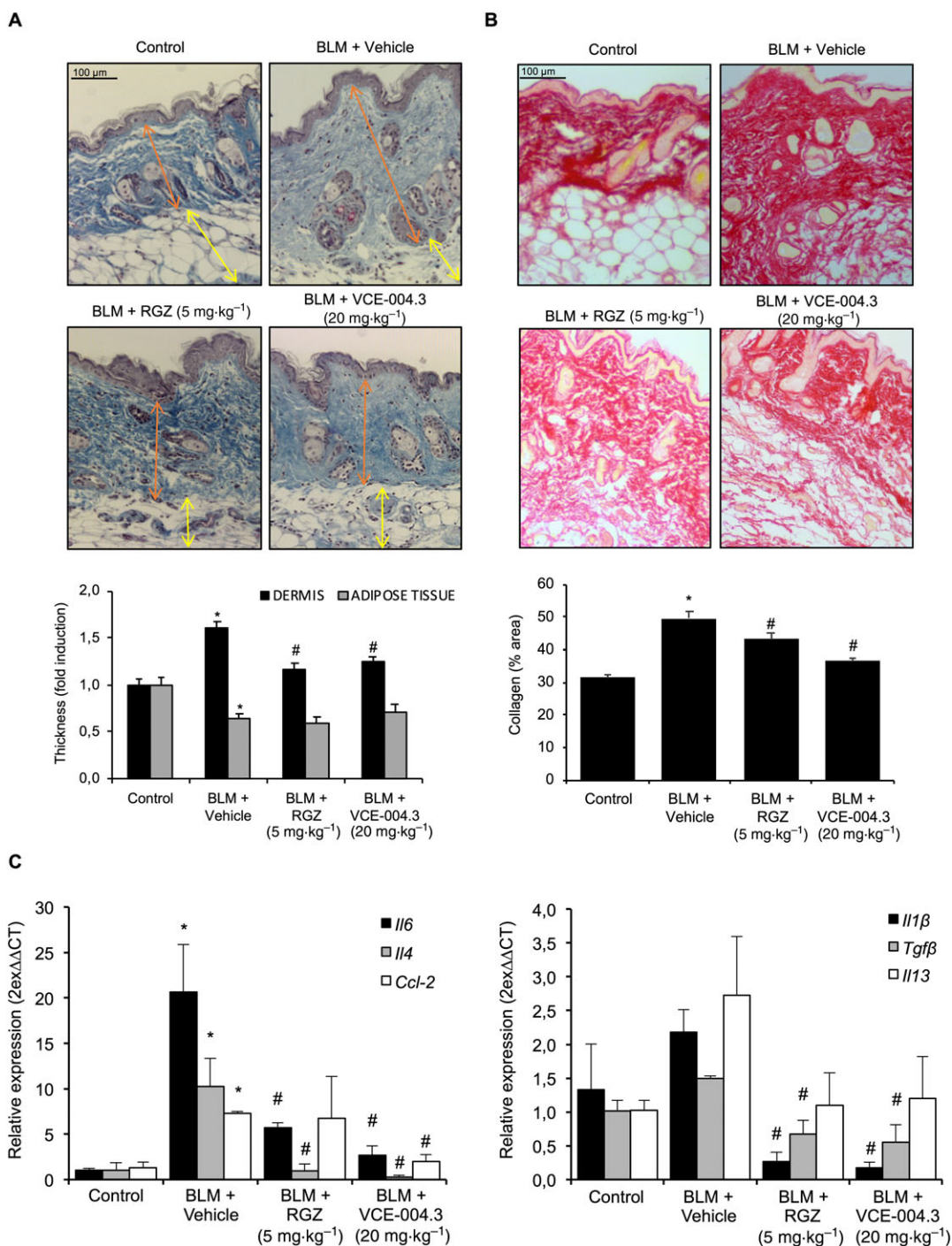


Figure 5

VCE-004.3 alleviated skin inflammation and collagen accumulation induced by BLM. Mice were injected with BLM for 3 weeks and treated in parallel with i.p. injections of RGZ, VCE-004.3 or vehicle. (A) Representative images of Masson's trichrome staining of skin sections and their respective measurement of the thickness of the layer of dermal and subcutaneous adipose tissue. (B) Representative images of collagen staining by picosirius red dye and their quantification. (C) Gene expression of profibrotic and pro-inflammatory genes including *Il-6*, *Tgfb*, *Il-4*, *Ccl2*, *Il-1β* and *Il-13* were measured by q-RT-PCR. Results are presented as mean ± SEM referred to control group ($n = 9$ animals per group). * $P < 0.05$ versus control; # $P < 0.05$ versus BLM-treated mice.

plus VCE-004.3 (20 mg·kg⁻¹ i.p.) or BLM plus VCE-004.3 (250 nM topically). Consistent with previous studies, dermal thickness increased more than twofold after 6 weeks of BLM

challenge in parallel with a strong reduction in the adipose tissue. Treatment for 3 weeks with VCE-004.3 in the absence of BLM did not influence the structures of the skin. In

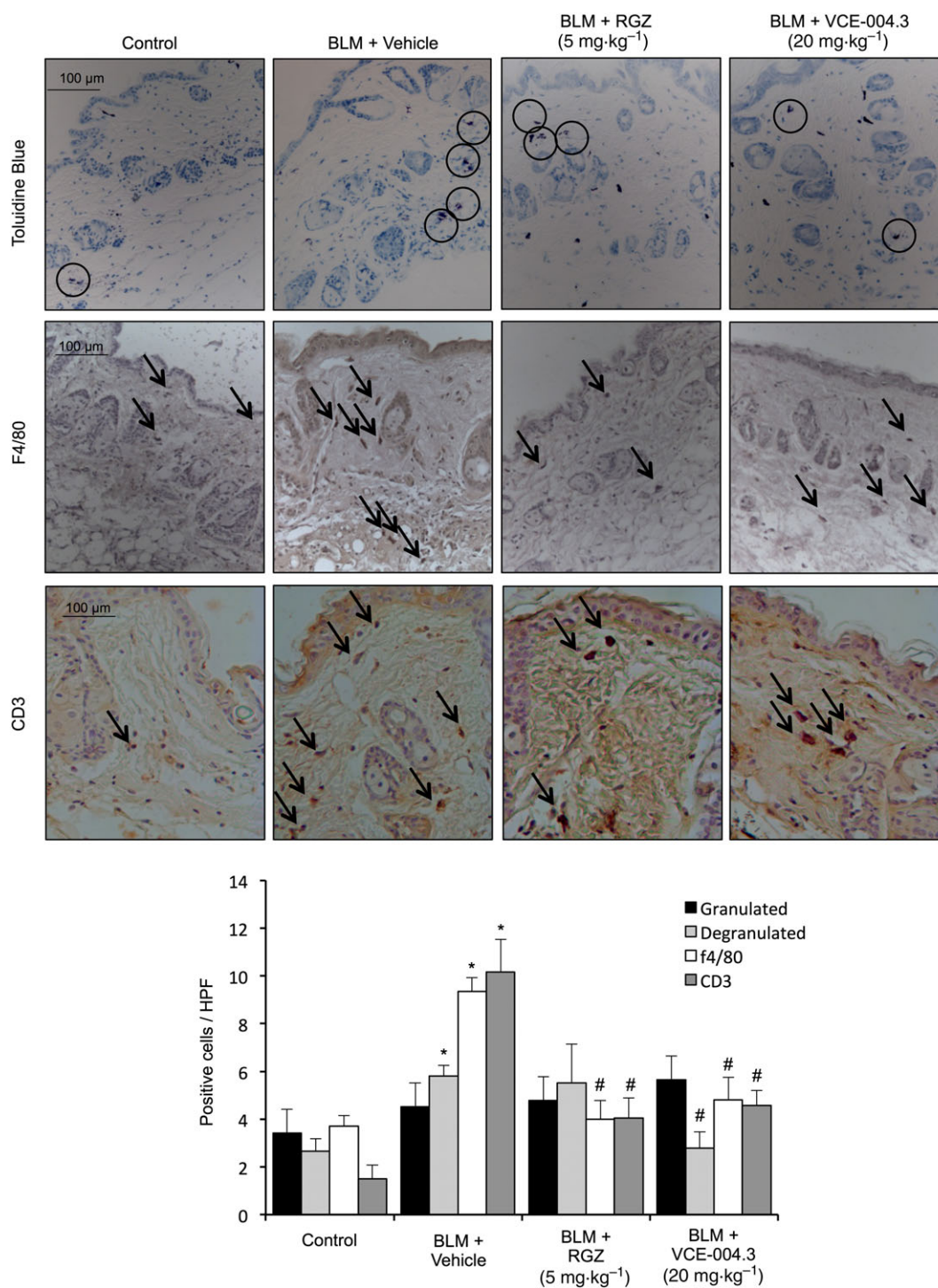


Figure 6

VCE-004.3 reduced inflammatory cell infiltration in the skin. Mice were injected with BLM for 3 weeks and treated in parallel with i.p. injections of RGZ, VCE-004.3 or vehicle. Representative images of the mast cell degranulation process are shown, as detected by toluidine blue staining and F4/80⁺ macrophages and CD3⁺ T-lymphocyte infiltration in the skin detected by immunostaining and their corresponding quantification ($n = 9$ animals per group). Results represent the mean \pm SEM. * $P < 0.05$ versus control; # $P < 0.05$ versus BLM-treated mice.

contrast, treatment with either RGZ or VCE-004.3 (i.p. or topical) of BLM-challenged mice significantly reversed dermal thickness, although they could restore the adipose layer thickness to the control level (Figure 9A). According to this

reduction of dermal thickness, RGZ and VCE-004.3 prevented collagen accumulation in the skin (Figure 9B). In a similar experiment, co-treatment with the CB₂ antagonist AM630 attenuated the effect of VCE-004.3 to a certain extent.

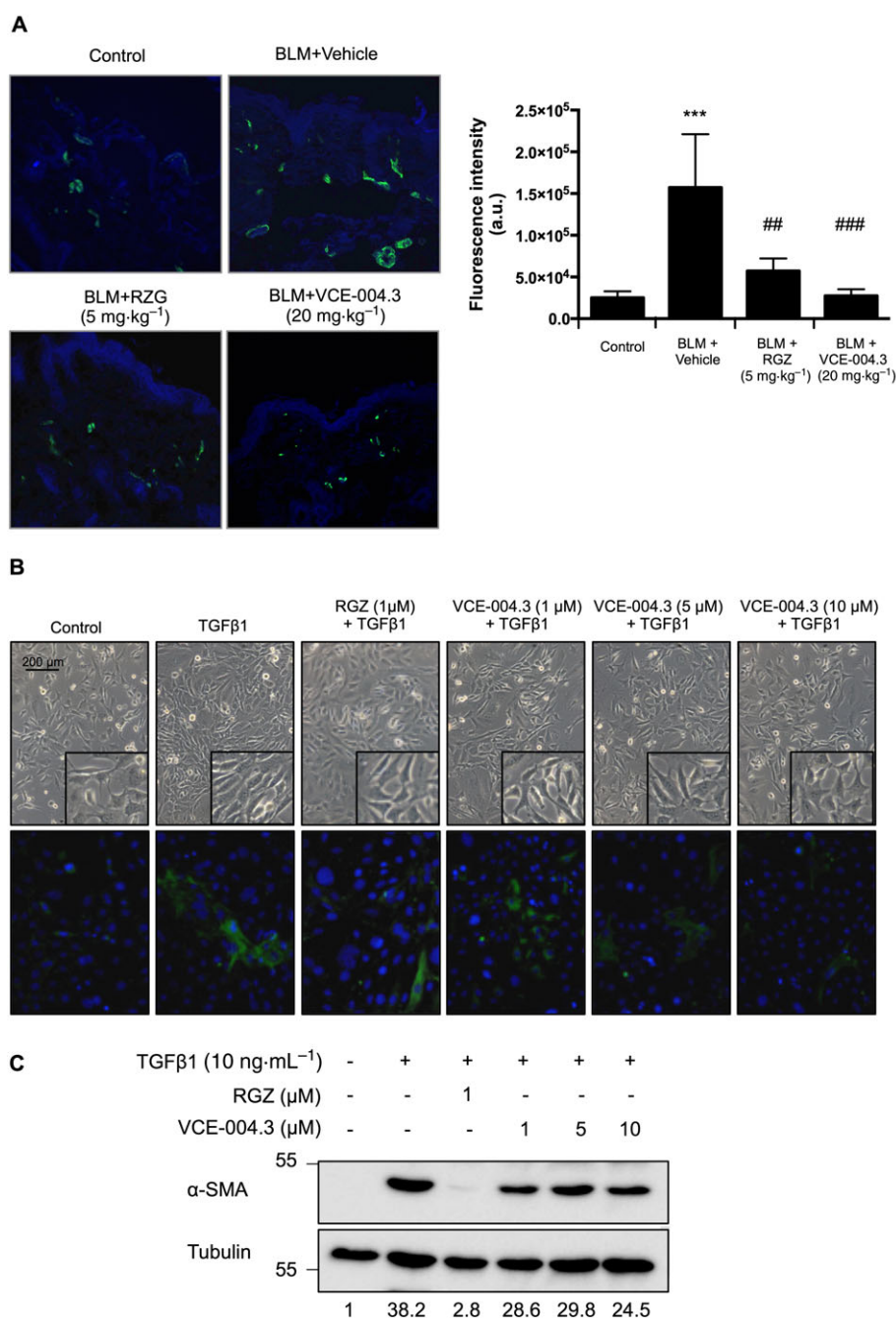


Figure 7

VCE-004.3 prevented BLM-induced myofibroblast accumulation and fibroblast to myofibroblast differentiation. (A) Mice were injected with BLM for 3 weeks and treated in parallel with i.p. injections of RGZ, VCE-004.3 or vehicle. Representative images of α -SMA⁺ cells in skin (green) detected by immunostaining and their corresponding quantification are shown ($n = 6$ animals per group). (B and C) NIH-3T3 differentiation into myofibroblasts. Cells were incubated in low serum conditions (1% FBS) for 24 h. Then, cells were pretreated with VCE-004.3 for 1 h and stimulated with TGFβ1 for 24 h (B, upper panel). Cells were immunostained for α -SMA (green) and their nuclei stained with DAPI (blue) (B, bottom panel). (C) α -SMA protein expression was determined by Western blot. Values under the gel indicate α -SMA protein signal intensities after normalization to tubulin signal intensities ($n = 5$).

However, the PPAR γ antagonist T0070907 could not block the effect of the compound, since no significant changes in either dermal thickness or collagen accumulation were observed when compared with VCE-004.3-treated animals

(Supporting Information Figure S2). This result confirmed that the biological activity of VCE-004.3 *in vivo* is mediated by targeting PPAR γ at the alternative binding site as well as its effect on CB₂ receptors.

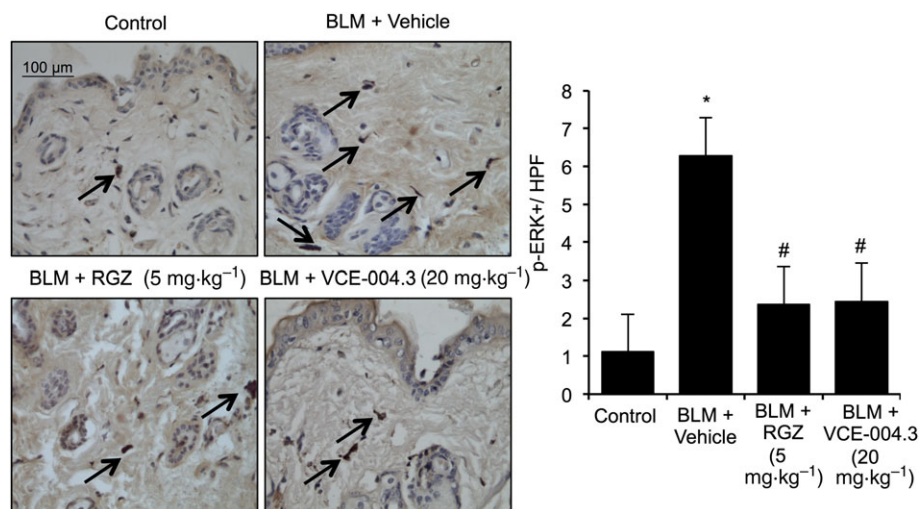


Figure 8

VCE-004.3 inhibited BLM-induced ERK1/2 phosphorylation *in vivo*. Mice were injected with BLM for 3 weeks and treated in parallel with i.p. injections of RGZ, VCE-004.3 or vehicle. Representative images of p-ERK⁺ cells detected by immunostaining and their respective quantification. Values are presented as mean ± SEM ($n = 9$ animals per group). * $P < 0.05$ versus control; # $P < 0.05$ versus BLM-treated mice.

The mRNA levels of *Il-4*, *Il-6* and *Tgfb* were also investigated in this model. Expression levels of *Il-6* were significantly reduced with all the pharmacological treatments. *Il-6* mRNA was increased in the fibrotic model, but to a much lesser extent than in the inflammatory model, indicating that the cytokine signature is different in the two approaches. Accordingly, *Il-4* mRNA in the skin was not significantly increased after 6 weeks of BLM challenge, but in any case, the expression levels were reduced in both RGZ and VCE-004.3 treated mice. The expression of *Tgfb* was strongly up-regulated in the BLM group, and this effect was partially inhibited in VCE-004.3 (i.p.) treated mice and significantly reduced after RGZ and topical VCE-004.3 treatments (Figure 9C).

Effect of VCE-004.3 on ERK1/2 activation and fibroblast migration

It is well accepted that autoantibodies could play a key role in the pathogenesis of SSc. Stimulatory autoantibodies targeting the PDGF receptor have been detected in 100% of SSc patients and demonstrated to trigger an intracellular cascade that involves ROS, Ha-Ras and ERK1/2 activation, eventually leading to fibroblast activation and increased collagen gene expression (Baroni *et al.*, 2006; Luchetti *et al.*, 2016). In addition, different studies have demonstrated that MAPKs are activated in response to fibrogenic stimuli and contribute to myofibroblast differentiation and function (Leask, 2012). To study the effect of VCE-004.3 on ERK1/2 phosphorylation, NHDFs were preincubated with the compound under investigation, and then stimulated with human recombinant PDGF-BB, or with IgG purified from patients diagnosed with lcSSc or dcSSc, with the steady state levels for total and phosphorylated ERK1/2 protein being analysed by Western blots. VCE-004.3 clearly prevented

ERK1/2 phosphorylation in all the condition tested (Figure 10A–C).

Migration of skin fibroblast plays a crucial role in SSc (Gilbane *et al.*, 2013), and we tested if the anti-fibrotic effect of VCE-004.3 could be associated with reduced fibroblast migration. Thus, NHDF cell monolayers were scratched, and the effect of VCE-004.3 on TGFβ1-induced wound healing was analysed over the time. Our results show that VCE-004.3 strongly inhibited the migration of fibroblasts induced by TGFβ1 (Figure 10D).

Discussion

We and others have previously investigated the anti-fibrotic effects of synthetic cannabinoids that activate both PPAR_γ and CB₂ receptors in animal models of skin fibrosis (Gonzalez *et al.*, 2012; del Rio *et al.*, 2016). In this study, we report for the first time that a novel CBD derivative, VCE-004.3, which is a dual PPAR_γ/CB₂ agonist that also behaves as a CB₁ antagonist, exhibits both anti-inflammatory and anti-fibrotic effects.

Glitazones like RGZ are full agonists of PPAR_γ (PPAR_γ-fa) that are widely used in clinical practice for glycaemic control. Nevertheless, this kind of PPAR_γ-fa may cause several adverse effects, including fluid retention, congestive heart failure and bladder cancer (Ciudin *et al.*, 2012). Accordingly, the search for PPAR_γ modulators (PPAR_γ-m) as safer alternatives to PPAR_γ-fa has grown, with the expectation of separating mechanism-associated side effects from insulin-sensitizing activity. It has been demonstrated that the level of activation of PPAR_γ is directly related to adipogenesis but not to insulin sensitivity (Doshi *et al.*, 2010). PPAR_γ-m can bind the receptor in a different manner than PPAR_γ-fa, leading conformational changes that alter coactivator recruitment (Doshi *et al.*, 2010). In this context, VCE-004.3 can be

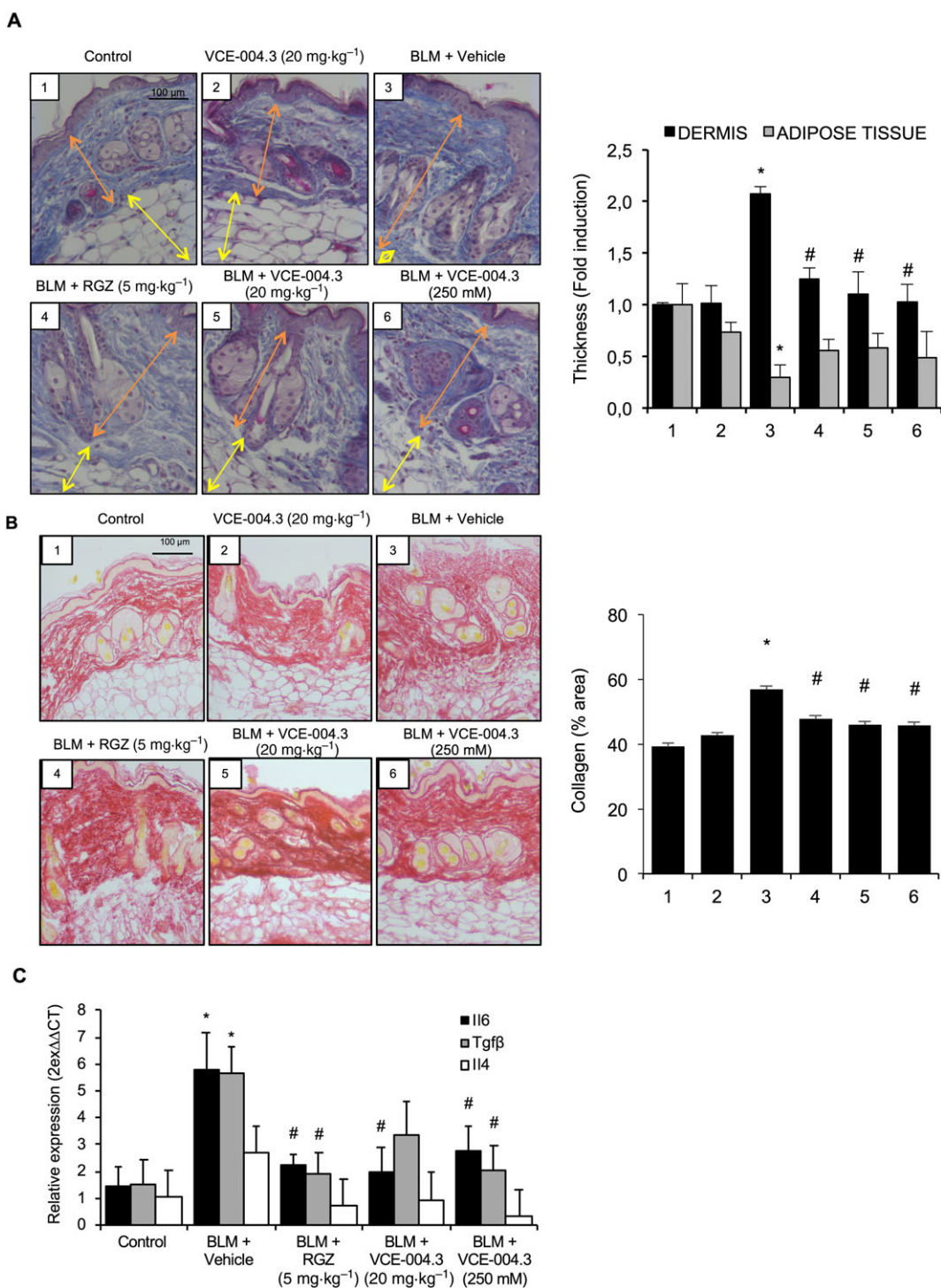


Figure 9

Systemic and topical treatment with VCE-004.3 reversed fibrosis in a BLM-induced model of established skin fibrosis. Mice were injected with BLM for 6 weeks and treated with the compound during the last 3 weeks of BLM challenge. (A) Representative images of Masson’s trichrome staining of skin sections and their respective measurements of the thickness of dermal and subcutaneous adipose layers. (B) Representative images of collagen staining by picosirius red dye and their quantification. (C) Expression of fibrosis-related genes in the skin. Values are presented as mean ± SEM (n = 9 animals per group). *P < 0.05 versus control; #P < 0.05 versus BLM-treated mice.

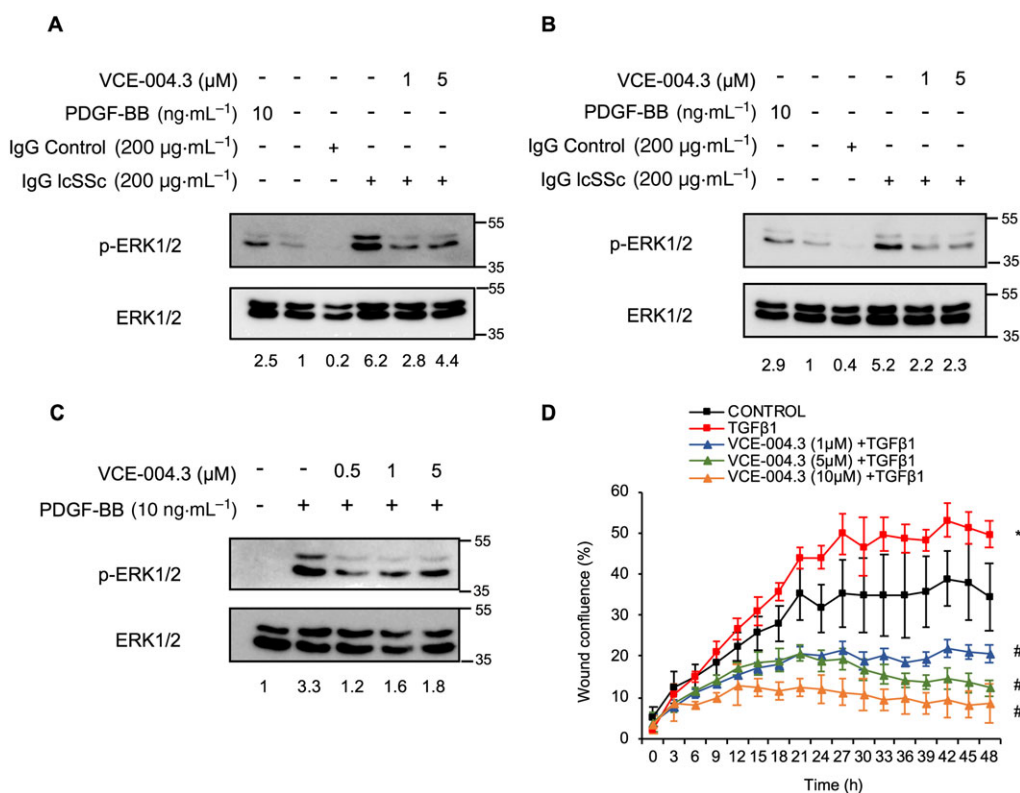


Figure 10

VCE-004.3 prevented stimulation of ERK signalling by SSc autoantibodies and fibroblast migration *in vitro*. NHDFs were serum-starved (1% FBS) for 24 h and then preincubated with VCE-004.3 for 1 h and stimulated with ISSc (A) or dSSc (B) IgG for 15 min. (C) NIH-3T3 cells were serum-starved (1% FBS) for 24 h and then preincubated with VCE-004.3 for 15 min and stimulated with PDGF-BB for 5 min. Protein expression was determined by Western blot, and values under the gel indicate mean fold induction of signal intensities. (D) NHDF monolayers were scratched and treated with VCE-004.3 at the indicated doses in the presence of TGF β 1. Results are presented as percentage of wound closure (confluence) \pm SD ($n = 5$). * $P < 0.05$ versus control; # $P < 0.05$ versus TGF β 1-treated cells.

considered as a PPAR γ -m, since it is less potent as an activator PPAR γ than RGZ, and is less adipogenic. Here, we showed that VCE-004.3 activates PPAR γ transcriptional activity and competes for the RGZ binding pocket, which is located within the PPAR γ LBP. However, the effect of VCE-004.3 on PPAR γ transactivation could not be blocked by T0070907 showing that both compounds bind simultaneously to distinct PPAR γ binding sites, as confirmed by docking studies. These results are consistent with previous studies that reported that covalent antagonists do not block ligands that interact with the alternate binding site (Hughes *et al.*, 2014). Moreover, synthetic PPAR γ agonists that bind to the alternate site induce PPAR γ -driven anti-diabetic activities (Hughes *et al.*, 2014). Thus, it was not unexpected to find that T0070907 did not prevent the anti-fibrotic response of VCE-004.3 in our *in vivo* studies. Since PPAR γ ligands that bind to canonical binding site are also effective in BLM-induced fibrosis (Wu *et al.*, 2009; Wei *et al.*, 2014), we can assume that, due to the versatile nature of the LBP of PPAR γ , PPAR γ -ms (partial agonist) are also effective at preventing inflammation and fibrosis.

It has been previously shown that the canonical pathway activated by TGF β drives the phosphorylation of SMADs that is upstream of the fibrogenic process (Walton *et al.*, 2017). Our results show that VCE-004.3 reduces

TGF β -induced SMAD2/3 transcriptional activation and collagen synthesis but does not affect SMAD2/3 phosphorylation. Since ligand-mediated PPAR γ activation does not interfere with the phosphorylation of SMADs, it is likely that VCE-004.3 competes with SMAD proteins for the interaction with p300 co-activator, thus preventing collagen synthesis induced by TGF β (Ghosh *et al.*, 2009). However, other TGF β -dependent signalling pathways such as the Ras/MEK/ERK cascade have also been suggested to contribute to SSc pathogenesis (Leask, 2012). VCE-004.3 also down-regulates ERK1/2 signalling, a major pathway controlling cell growth, proliferation, migration, apoptosis and myofibroblast differentiation (McCubrey *et al.*, 2007). Indeed, hyperactivation of ERK1/2 was observed in fibroblasts from SSc patients, and MEK/ERK signalling is required for α -SMA stress fibre assembly (Chen *et al.*, 2011). Interestingly, a recent report has shown that skin fibroblasts express CB $_2$ receptors and that these are further up-regulated under inflammatory conditions (Bort *et al.*, 2017). It is therefore possible that VCE-004.3 inhibits ERK1/2 activation both *in vitro* and *in vivo* by acting directly through CB $_2$ receptors. Accordingly, the anti-fibrotic activity of VCE-004.3 *in vivo* was partially prevented by the CB $_2$ antagonist AM630.

The earliest events of SSc include obliterative vasculopathy, which induces inflammation and autoimmunity. Indeed, in early dcSSc, the dermis exhibits inflammatory infiltrates mainly composed of monocytes and activated lymphocytes (Varga and Abraham, 2007). Accordingly, we used a model characterized by early inflammation induced by 3 weeks of BLM administration in which treatment with the compound is carried out in parallel with the BLM injections (Gonzalez *et al.*, 2012). Our data indicate that VCE-004.3 prevents dermal thickening as well as inflammatory cell infiltration and the expression of pro-inflammatory and profibrotic cytokines. Previous studies have shown that PPAR γ activation by RGZ mediates immunomodulatory effects that prevent BLM-induced skin fibrosis (Wu *et al.*, 2009). Moreover, macrophage activation as well as T-cell proliferation are also regulated by PPAR γ activation (Clark *et al.*, 2000; Harris and Phipps, 2001). Indeed, activators of PPAR γ and CB $_2$ receptors inhibited M1 polarization and influenced macrophage M2 differentiation (Bouhlef *et al.*, 2007; Guillot *et al.*, 2014). Therefore, it is conceivable that PPAR γ activation and modulation of the cannabinoid system by VCE-004.3 could limit leukocyte infiltration and macrophage activation in the skin after BLM administration (Akhmetshina *et al.*, 2009; Marquart *et al.*, 2010).

The BLM-induced model of SSc is also useful to evaluate the progression from an inflammatory process to a fibrotic state. In this model, skin fibrosis is measured by determining dermal thickness, myofibroblast counts and collagen content, assessed by the hydroxyproline assay. Alternatively, the content of collagen in skin biopsies can be also evaluated by picrosirius staining, a semi-quantitative method, since a highly significant correlation between picrosirius staining and the results of hydroxyproline assays used to measure skin collagen have recently been found (Caetano *et al.*, 2016). Progressive fibrosis of the skin and other internal organs caused by excessive accumulation of collagen and other ECM is one of the three main hallmarks of SSc (Pattanaik *et al.*, 2015). Many compounds that have been tested using the BLM model were investigated in a preventive schedule to see if an anti-inflammatory agent can hinder the subsequent fibrosis. In the event, treatment with VCE-004.3 (topical and i.p.) could reduce dermal thickness and collagen content as well as the expression of cytokines involved in collagen production after the development of fibrosis, thus alleviating the previously established damage. CB $_1$ and CB $_2$ receptors have been shown to play opposite roles in experimental models of skin fibrosis. While CB $_1$ receptor activation has a detrimental effect on the disease, the genetic or pharmacological inactivation of this receptor alleviates skin fibrosis. In addition, CB $_2$ agonists have been shown to prevent BLM-induced fibrosis (Akhmetshina *et al.*, 2009; Marquart *et al.*, 2010; Gonzalez *et al.*, 2012; del Rio *et al.*, 2016). Thus, VCE-004.3 may have a beneficial effect on skin fibrosis by acting as a dual CB $_1$ antagonist and CB $_2$ agonist. While the CB $_2$ agonism effect on BLM-induced skin fibrosis has been confirmed using AM630, the potential CB $_1$ antagonism requires further research. We found that VCE-004.3 binds to CB $_1$ receptors with relatively low affinity but inhibits CB $_1$ -dependent cAMP

signalling with a potency similar to other CB $_1$ antagonists. This Janus-behaviour (Dhopeswarkar *et al.*, 2017) could, in principle, be due to either to binding to a different site to [3 H]-CP55940 or to it behaving as a potential negative allosteric modulator. Experiments are on course to elucidate the mechanism of action of VCE-004.3 on the functionality of CB $_1$ receptors.

As in many autoimmune diseases, beta cell activation and generation of autoantibodies against different targets are also present in SSc patients, and this plays a critical role in the pathogenesis of the disease. Among others, agonistic PDGF receptor autoantibodies have been shown to change fibroblast phenotype into SSc features through Ha-Ras-ERK1/2 and ROS cascades (Baroni *et al.*, 2006). In addition, the inhibiting the activation of MAPKs has been shown to suppress the progression of fibrosis (Galuppo *et al.*, 2011). Treatment with VCE-004.3 prevented ERK1/2 activation in normal fibroblasts after they were exposed to stimulatory autoantibodies isolated from lcSSc and dcSSc patients, indicating that the anti-fibrotic effects of VCE-004.3 may be also mediated by ERK1/2. Interestingly, the presence of autoantibodies has been also demonstrated in the BLM model (Yamamoto, 2006), and it is, therefore, possible that VCE-004.3 inhibits ERK1/2 activation *in vivo* by targeting both TGF β - and autoantibody-induced ERK1/2 phosphorylation.

Finally, the transdermal administration of cannabinoids is now well established (Lodzki *et al.*, 2003; Valiveti *et al.*, 2004), and in this study, we have shown that topical application of VCE-004.3 also inhibited BLM-induced skin fibrosis; therefore, this compound could be also formulated for the treatment of localized forms of cutaneous fibrosis.

Cannabinoids like CBD are multitarget compounds and many semisynthetic derivatives have been designed to improve the bioactivities and druggability of the natural products. In this context, VCE-004.3 is a novel cannabinoid derivative that acts as a dual PPAR γ /CB $_2$ agonist and as a negative modulator of CB $_1$ receptors. Because of this, it qualifies as a candidate for the development of novel therapies against different forms of scleroderma.

Acknowledgements

This work was partially supported by the MINECO grant RTC-2015-3364 cofounded by the European Development Regional Fund in the Framework of the Operative Program 'Reinforcement of research, technological development and innovation'. E.M. was also supported by the MINECO grant SAF2014-53763-P. B.P. is a predoctoral fellow supported by the i-PFIS program, Instituto de Salud Carlos III (IFI15/00022; European Social Fund "investing in your future").

Author contributions

C.D.R., I.C. and E.M. contributed to the conception and design of the study. C.D.R., I.C., B.P., C.N., A.G.M. and M.L.B.

performed *in vitro* and *in vivo* experiments. C.D.R. and B.P. conducted the statistical analysis. M.G.C. and J.F.R. performed the binding studies. R.O.C., C.P.S. and C.L.P. selected patients and isolated IgG from plasma. C.P. and M.A.C. performed the *in silico* analysis. G.A. supervised the chemical synthesis of VCE-004.3. C.D.R. and E.M. wrote the manuscript. All the authors contributed to the analysis and interpretation of data, critically reviewed and approved the manuscript.

Conflict of interest

The authors declare no conflicts of interest.

Declaration of transparency and scientific rigour

This Declaration acknowledges that this paper adheres to the principles for transparent reporting and scientific rigour of preclinical research recommended by funding agencies, publishers and other organisations engaged with supporting research.

References

Akhmetshina A, Dees C, Busch N, Beer J, Sarter K, Zwerina J *et al.* (2009). The cannabinoid receptor CB₂ exerts antifibrotic effects in experimental dermal fibrosis. *Arthritis Rheum* 60: 1129–1136.

Alexander SPH, Cidrowski JA, Kelly E, Marrion NV, Peters JA, Faccenda E *et al.* (2017a). The Concise Guide to PHARMACOLOGY 2017/18: Nuclear hormone receptors. *Br J Pharmacol* 174: S208–S224.

Alexander SPH, Christopoulos A, Davenport AP, Kelly E, Marrion NV, Peters JA *et al.* (2017b). The Concise Guide to PHARMACOLOGY 2017/18: G protein-coupled receptors. *Br J Pharmacol* 174: S17–S129.

Alexander SPH, Fabbro D, Kelly E, Marrion NV, Peters JA, Faccenda E *et al.* (2017c). The Concise Guide to PHARMACOLOGY 2017/18: Enzymes. *Br J Pharmacol* 174: S272–S359.

Avouac J (2014). Mouse model of experimental dermal fibrosis: the bleomycin-induced dermal fibrosis. *Methods Mol Biol* 1142: 91–98.

Bae KH, Seo JB, Jung YA, Seo HY, Kang SH, Jeon HJ *et al.* (2017). Lobeglitazone, a novel peroxisome proliferator-activated receptor γ agonist, attenuates renal fibrosis caused by unilateral ureteral obstruction in mice. *Endocrinol Metab (Seoul)* 32: 115–123.

Baroni SS, Santillo M, Bevilacqua F, Luchetti M, Spadoni T, Mancini M *et al.* (2006). Stimulatory autoantibodies to the PDGF receptor in systemic sclerosis. *N Engl J Med* 354: 2667–2676.

Baugh EH, Lyskov S, Weitzner BD, Gray JJ (2011). Real-time PyMOL visualization for Rosetta and Pyrosetta. *PLoS One* 6: e21931.

Beyer C, Schett G, Distler O, Distler JH (2010). Animal models of systemic sclerosis: prospects and limitations. *Arthritis Rheum* 62: 2831–2844.

Bort A, Alvarado-Vazquez PA, Moracho-Vilrriales C, Virga KG, Gumina G, Romero-Sandoval A *et al.* (2017). Effects of JWH015 in

cytokine secretion in primary human keratinocytes and fibroblasts and its suitability for topical/transdermal delivery. *Mol Pain* 13 1744806916688220.

Bouchard JF, Lepicier P, Lamontagne D (2003). Contribution of endocannabinoids in the endothelial protection afforded by ischemic preconditioning in the isolated rat heart. *Life Sci* 72: 1859–1870.

Bouhrel MA, Derudas B, Rigamonti E, Dievart R, Brozek J, Haulon S *et al.* (2007). PPAR γ activation primes human monocytes into alternative M2 macrophages with anti-inflammatory properties. *Cell Metab* 6: 137–143.

Caetano GF, Fronza M, Leite MN, Gomes A, Frade MA (2016). Comparison of collagen content in skin wounds evaluated by biochemical assay and by computer-aided histomorphometric analysis. *Pharm Biol* 54: 2555–2559.

Chen Y, Leask A, Abraham DJ, Kennedy L, Shi-Wen X, Denton CP *et al.* (2011). Thrombospondin 1 is a key mediator of transforming growth factor β -mediated cell contractility in systemic sclerosis via a mitogen-activated protein kinase (MEK)/extracellular signal-regulated kinase (ERK)-dependent mechanism. *Fibrogenesis Tissue Repair* 4: 9.

Ciudin A, Hernandez C, Simo R (2012). Update on cardiovascular safety of PPAR γ agonists and relevance to medicinal chemistry and clinical pharmacology. *Curr Top Med Chem* 12: 585–604.

Clark RB (2002). The role of PPARs in inflammation and immunity. *J Leukoc Biol* 71: 388–400.

Clark RB, Bishop-Bailey D, Estrada-Hernandez T, Hla T, Puddington L, Padula SJ (2000). The nuclear receptor PPAR γ and immunoregulation: PPAR γ mediates inhibition of helper T cell responses. *J Immunol* 164: 1364–1371.

Curtis MJ, Alexander S, Cirino G, Docherty JR, George CH, Giembycz MA *et al.* (2018). Experimental design and analysis and their reporting II: updated and simplified guidance for authors and peer reviewers. *Br J Pharmacol* 175: 987–993.

Dantas AT, Pereira MC, De Melo Rego MJ, Darocha LF Jr, Pitta Ida R, Marques CD *et al.* (2015). The role of PPAR γ in systemic sclerosis. *PPAR Res* 2015: 124624.

del Rio C, Navarrete C, Collado JA, Bellido ML, Gomez-Canas M, Pazos MR *et al.* (2016). The cannabinoid quinol VCE-004.8 alleviates bleomycin-induced scleroderma and exerts potent antifibrotic effects through peroxisome proliferator-activated receptor- γ and CB₂ pathways. *Sci Rep* 6 21703.

Dhopeswarkar A, Murataeva N, Makriyannis A, Straiker A, Mackie K (2017). Two Janus cannabinoids that are both CB₂ agonists and CB₁ antagonists. *J Pharmacol Exp Ther* 360: 300–311.

Doshi LS, Brahma MK, Bahirat UA, Dixit AV, Nemmani KV (2010). Discovery and development of selective PPAR γ modulators as safe and effective antidiabetic agents. *Expert Opin Investig Drugs* 19: 489–512.

Fineschi S, Goffin L, Rezzonico R, Cozzi F, Dayer JM, Meroni PL *et al.* (2008). Antifibroblast antibodies in systemic sclerosis induce fibroblasts to produce profibrotic chemokines, with partial exploitation of toll-like receptor 4. *Arthritis Rheum* 58: 3913–3923.

Galli A, Crabb DW, Ceni E, Salzano R, Mello T, Svegliati-Baroni G *et al.* (2002). Antidiabetic thiazolidinediones inhibit collagen synthesis and hepatic stellate cell activation *in vivo* and *in vitro*. *Gastroenterology* 122: 1924–1940.

- Galuppo M, Esposito E, Mazzon E, Di Paola R, Paterniti I, Impellizzeri D *et al.* (2011). MEK inhibition suppresses the development of lung fibrosis in the bleomycin model. *Naunyn Schmiedeberg's Arch Pharmacol* 384: 21–37.
- Garcia-Gonzalez E, Selvi E, Balistreri E, Lorenzini S, Maggio R, Natale MR *et al.* (2009). Cannabinoids inhibit fibrogenesis in diffuse systemic sclerosis fibroblasts. *Rheumatology (Oxford)* 48: 1050–1056.
- Ghosh AK, Bhattacharyya S, Wei J, Kim S, Barak Y, Mori *et al.* (2009). Peroxisome proliferator-activated receptor- γ abrogates Smad-dependent collagen stimulation by targeting the p300 transcriptional coactivator. *FASEB J* 23: 2968–2977.
- Gilbane AJ, Denton CP, Holmes AM (2013). Scleroderma pathogenesis: a pivotal role for fibroblasts as effector cells. *Arthritis Res Ther* 15: 215.
- Gonzalez EG, Selvi E, Balistreri E, Akhmetshina A, Palumbo K, Lorenzini S *et al.* (2012). Synthetic cannabinoid ajulemic acid exerts potent antifibrotic effects in experimental models of systemic sclerosis. *Ann Rheum Dis* 71: 1545–1551.
- Guillot A, Hamdaoui N, Bizy A, Zoltani K, Souktani R, Zafrani ES *et al.* (2014). Cannabinoid receptor 2 counteracts interleukin-17-induced immune and fibrogenic responses in mouse liver. *Hepatology* 59: 296–306.
- Harding SD, Sharman JL, Faccenda E, Southan C, Pawson AJ, Ireland S *et al.* (2018). The IUPHAR/BPS guide to pharmacology in 2018: updates and expansion to encompass the new guide to immunopharmacology. *Nucl Acids Res* 46: D1091–D1106.
- Harris SG, Phipps RP (2001). The nuclear receptor PPAR γ is expressed by mouse T lymphocytes and PPAR γ agonists induce apoptosis. *Eur J Immunol* 31: 1098–1105.
- Ho KT, Reveille JD (2003). The clinical relevance of autoantibodies in scleroderma. *Arthritis Res Ther* 5: 80–93.
- Hughes TS, Giri PK, De Vera IM, Marciano DP, Kuruvilla DS, Shin Y *et al.* (2014). An alternate binding site for PPAR γ ligands. *Nat Commun* 5: 3571.
- Katchan V, David P, Shoenfeld Y (2016). Cannabinoids and autoimmune diseases: a systematic review. *Autoimmun Rev* 15: 513–528.
- Kayser C, Fritzler MJ (2015). Autoantibodies in systemic sclerosis: unanswered questions. *Front Immunol* 6: 167.
- Kilkenny C, Browne W, Cuthill IC, Emerson M, Altman DG (2010). Animal research: reporting *in vivo* experiments: the ARRIVE guidelines. *Br J Pharmacol* 160: 1577–1579.
- Leask A (2012). MEK/ERK inhibitors: proof-of-concept studies in lung fibrosis. *J Cell Commun Signal* 6: 59–60.
- Lodzki M, Godin B, Rakou L, Mechoulam R, Gallily R, Touitou E (2003). Cannabidiol-transdermal delivery and anti-inflammatory effect in a murine model. *J Control Release* 93: 377–387.
- Luchetti MM, Moroncini G, Jose Escamez M, Svegliati Baroni S, Spadoni T, Grieco A *et al.* (2016). Induction of scleroderma fibrosis in skin-humanized mice by administration of anti-platelet-derived growth factor receptor agonistic autoantibodies. *Arthritis Rheumatol* 68: 2263–2273.
- Marangoni RG, Korman BD, Wei J, Wood TA, Graham LV, Whitfield ML *et al.* (2015). Myofibroblasts in murine cutaneous fibrosis originate from adiponectin-positive intradermal progenitors. *Arthritis Rheumatol* 67: 1062–1073.
- Marquart S, Zerr P, Akhmetshina A, Palumbo K, Reich N, Tomcik M *et al.* (2010). Inactivation of the cannabinoid receptor CB1 prevents leukocyte infiltration and experimental fibrosis. *Arthritis Rheum* 62: 3467–3476.
- McCubrey JA, Steelman LS, Chappell WH, Abrams SL, Wong EW, Chang F *et al.* (2007). Roles of the Raf/MEK/ERK pathway in cell growth, malignant transformation and drug resistance. *Biochim Biophys Acta* 1773: 1263–1284.
- McGrath JC, Lilley E (2015). Implementing guidelines on reporting research using animals (ARRIVE etc.): new requirements for publication in BJP. *Br J Pharmacol* 172: 3189–3193.
- Mihai C, Tervaert JW (2010). Anti-endothelial cell antibodies in systemic sclerosis. *Ann Rheum Dis* 69: 319–324.
- Milam JE, Keshamouni VG, Phan SH, Hu B, Gangireddy SR, Hogaboam CM *et al.* (2008). PPAR- γ agonists inhibit profibrotic phenotypes in human lung fibroblasts and bleomycin-induced pulmonary fibrosis. *Am J Physiol Lung Cell Mol Physiol* 294: L891–L901.
- Morris GM, Huey R, Lindstrom W, Sanner MF, Belew RK, Goodsell DS *et al.* (2009). AutoDock4 and AutoDockTools4: automated docking with selective receptor flexibility. *J Comput Chem* 30: 2785–2791.
- Pacher P, Batkai S, Kunos G (2006). The endocannabinoid system as an emerging target of pharmacotherapy. *Pharmacol Rev* 58: 389–462.
- Pattanaik D, Brown M, Postlethwaite BC, Postlethwaite AE (2015). Pathogenesis of systemic sclerosis. *Front Immunol* 6: 272.
- Pistis M, O'Sullivan SE (2017). The role of nuclear hormone receptors in cannabinoid function. *Adv Pharmacol* 80: 291–328.
- Ragusa G, Gomez-Canas M, Morales P, Hurst DP, Deligia F, Pazos R *et al.* (2015). Synthesis, pharmacological evaluation and docking studies of pyrrole structure-based CB₂ receptor antagonists. *Eur J Med Chem* 101: 651–667.
- Rajapaksha H, Bhatia H, Wegener K, Petrovsky N, Bruning JB (2017). X-ray crystal structure of rivoglitazone bound to PPAR γ and PPAR subtype selectivity of TZDs. *Biochim Biophys Acta* 1861: 1981–1991.
- Ruzehaji N, Frantz C, Ponsoye M, Avouac J, Pezet S, Guilbert T *et al.* (2016). Pan PPAR agonist IVA337 is effective in prevention and treatment of experimental skin fibrosis. *Ann Rheum Dis* 75: 2175–2183.
- Shi Y, Massague J (2003). Mechanisms of TGF- β signaling from cell membrane to the nucleus. *Cell* 113: 685–700.
- Trott O, Olson AJ (2010). AutoDock Vina: improving the speed and accuracy of docking with a new scoring function, efficient optimization, and multithreading. *J Comput Chem* 31: 455–461.
- Valiveti S, Hammell DC, Earles DC, Stinchcomb AL (2004). Transdermal delivery of the synthetic cannabinoid WIN 55,212-2: *in vitro/in vivo* correlation. *Pharm Res* 21: 1137–1145.
- Varga J, Abraham D (2007). Systemic sclerosis: a prototypic multisystem fibrotic disorder. *J Clin Invest* 117: 557–567.
- Walton KL, Johnson KE, Harrison CA (2017). Targeting TGF- β mediated SMAD signaling for the prevention of fibrosis. *Front Pharmacol* 8: 461.
- Wei J, Zhu H, Komura K, Lord G, Tomcik M, Wang W *et al.* (2014). A synthetic PPAR- γ agonist triterpenoid ameliorates experimental fibrosis: PPAR- γ -independent suppression of fibrotic responses. *Ann Rheum Dis* 73: 446–454.

Wolf LK (2009). New software and websites for the chemical enterprise. *Chem Eng News* 87: 48.

Wu M, Melichian DS, Chang E, Warner-Blankenship M, Ghosh AK, Varga J (2009). Rosiglitazone abrogates bleomycin-induced scleroderma and blocks profibrotic responses through peroxisome proliferator-activated receptor- γ . *Am J Pathol* 174: 519–533.

Yamamoto T (2006). The bleomycin-induced scleroderma model: what have we learned for scleroderma pathogenesis? *Arch Dermatol Res* 297: 333–344.

Yamamoto T, Takagawa S, Katayama I, Yamazaki K, Hamazaki Y, Shinkai H *et al.* (1999). Animal model of sclerotic skin. I: local injections of bleomycin induce sclerotic skin mimicking scleroderma. *J Invest Dermatol* 112: 456–462.

Supporting Information

Additional supporting information may be found online in the Supporting Information section at the end of the article.

<https://doi.org/10.1111/bph.14450>

Figure S1 Effect of VCE-004.3 on MSC differentiation into adipocytes. (A) MSC underwent adipocytic differentiation in the presence of VCE-004.3 or RGZ as positive control. Representative images showing OilRed O staining (upper panel) and cell number (bottom left) and Oilred positive cells (bottom right) were counted. (B) Gene expression of PPAR- γ 2, ADIPOQ and CEBPA in MSCs differentiated for 14 days. Data represent the percentage of increase over AM considered as the 100% of adipogenic induction ($n = 5$) * $P < 0.05$ versus AM. **Figure S2** Pretreatment with the CB2 antagonist AM630 but not the PPAR γ antagonist T007907 partially abrogated the effect of VCE-004.3 on BLM-induced chronic model of SSc. Mice were injected with BLM for six weeks and treated with the compound in the presence of either AM630 or T007907 during the last three weeks of BLM challenge. A. Representative images of Masson's trichrome staining of skin sections and their respective measurement of dermal and subcutaneous adipose layer thickness. B. Representative images of picosirius red dye in mice skin and their quantification. Values are represented as mean \pm SEM ($n = 9$ animals per group). * $P < 0.05$ versus control; # $P < 0.05$ versus BLM-treated mice; † $P < 0.05$ versus BLM + VCE-004.3.